Spherical Scanning Measurement Challenge for Future Millimeter Wave Applications

F. Ferrero, Y. Benoit, L. Brochier, J. Lanteri,
J-Y Dauvignac, C. Migliaccio
University Nice Sophia Antipolis, CNRS, LEAT
Sophia Antipolis, France
Fabien.ferrero@unice.fr

S.F. Gregson
Nearfield Systems Inc.
19730 Magellan Drive,
Torrance, CA 90502-1104 USA

***Abstract*—A specific set-up for probe-fed antenna pattern measurements with an articulated arm has been developed with a 500mm AUT-probe distance. This paper will give an example of far-field measurement and highlight its advantages and limitations. A near-field approach to filter the probe effect is investigated. First measurement results, including amplitude and phase patterns, will be presented. Phase data will be leveraged to develop post-processing techniques to filter probe and environmental effects.**

I. INTRODUCTION

With the advent of silicon technologies, millimeter waves are becoming really attractive for consumer applications. Measurements related to millimeter wave (MMW) are very challenging because of the very small wavelength and large space attenuation. In order to design an efficient radiating system, antennas need to be placed as close as possible to the radiofrequency chip. Antennas can be directly fabricated on Silicon but this Antenna on Chip (AoC) approach suffers from efficiency issue because of the loss of the silicon substrate. This type of radiating element is the most difficult to measure, as the RF probe and the antenna are in on the same side.

A second solution is the antenna in package (AiP) approach where the silicon die is connected to the package carrier using flip-chip technology. With this solution, the radiating part and the chip could be placed on different sides, which facilitate measurements.

To measure AoC or AiP antenna, classical waveguide or coaxial connectors are not an option because an additional transition would be needed and it will strongly impact the radiation of the Antenna Under Test (AUT). Thus, this type of antenna must be connected using microelectronic RF probe technology on the ground-signal-ground (GSG) pad of the antenna with the AUT being fixed during measurement so as to provide a stable electrical connection.

Several set-ups have been proposed for probe fed antenna measurements. Most of the set-ups are using far-field spherical scanners [1-2]. This type of amplitude-only measurement suffers from scattering effect from the RF probe. Moreover, advanced processing techniques for near-field measurement, determination of phase center or holographic analysis are not possible. To overcome this limit, some research groups have proposed 2D-scanner with near-field acquisition [3-4]. An interesting hybrid solution user a robotic arm has been recently proposed in [5]. Recently, MMW spherical near-field has been studied to improve AUT measurements [6-7]. This type of system solution necessitates the use of a very accurate mechanical scanner combined with a very stable guided wave-path.

II. SET-UP DESCRIPTION

A. *Spherical scanning mechanics*

Considering all the different constraints related to probe fed measurements, a 3-axis scanner with a fixed AUT has been designed by NSI and can be seen presented in Figure 1.

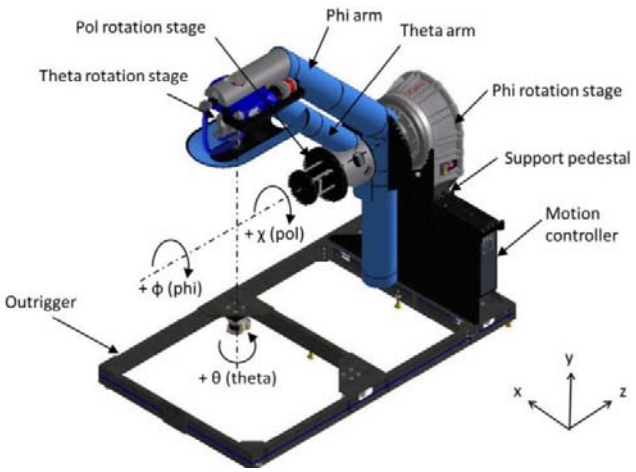

Figure 1. NSI-700S-360 Articulating 3-axis spherical near-field scanner

This robotic positioning system consists of a high-capacity 500 mm rotational positioner mounted on a large floor stand. This positioner defines the horizontal ϕ-axis of rotation. A second rotation stage is attached to this stage at an angle of 90° to the ϕ-axis and this forms the θ-axis of a conventional right handed polar spherical coordinate system. A third rotary stage is attached to the θ-stage again at an angle of 90° to the θ-axis and this forms the χ-axis. The combined motion of the θ and ϕ stages enables the probe tip to trace out a trajectory across the surface of a conceptual spherical surface centered about the

intersection of those orthogonal axes and whose definition is in accordance with standard SNF theory.

The spherical scanner structural and positioning performance data can be obtained from laser tracker dimensional measurements. These results allow one to establish a perturbed (θ', ϕ', r') grid, based on a regular (θ, ϕ, r) SNF grid. For the scanner shown in Figure.1, the total region of motion is practically limited to $-150° \le \theta \le 150°$ and $-180 \le \phi \le 180°$ by the AUT support stand, described below. It should be noted that these limitations are determined by the requirement to locate an AUT support in the keep-out region as the each of the individual positioners is capable of 360° motion. Results obtained for r' as a function of (θ, ϕ) are depicted below in Figure 2 in the form of a false color virtual 3D surface. Radial distance variation measured was less than ±1.2 mm over the spherical surface. Based on the result of the measurement radius r' a corresponding electrical phase correction pattern can be generated at each frequency of interest. This phase correction can then be applied to the measured SNF data as a first order correction term in an attempt to remove the phase impact of the structural variation. This correction is referred to as R-correction below. Although a similar correction can be considered for angular uncertainties, that was not implemented here as these are typically found to be a second order effect.

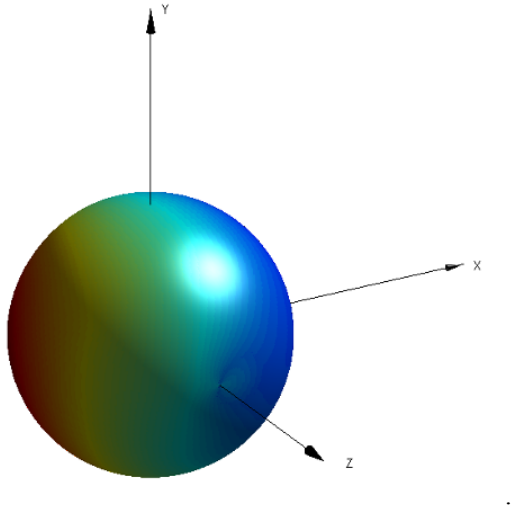

Figure 2. Scanner radius r' shown in scanner coordinate system. Here, the RMS radius variation was < 0.6 mm with the maximum variation being < ±1.2 mm.

B. *AUT probing system*

First, an additional support is added to the spherical set-up to support the AUT as shown in Figure 3. The AUT stand is mechanically connected to the base of the spherical system to guarantee an accurate positioning of the system. AUT holder is highly critical for probe-fed antenna system. Considering microelectronic wafer measurement, RF probing systems are usually done with the Device Under Test (DUT) placed on a non-resonant chuck made with metallic material. This type of holder has a strong impact on antenna radiation measurements. In this work, a specific antenna holder has been designed to limit as much as possible this interaction with the AUT. A low-permittivity foam material has been manufactured as shown in [1]. This approach is adding some difficulty to the probing operation as the mechanical holder is more flexible than classical metallic holder. Due to the small physical size of the electrical probes and antenna pads a moveable, high resolution microscope is used for an accurate probing operation (Figure 4).

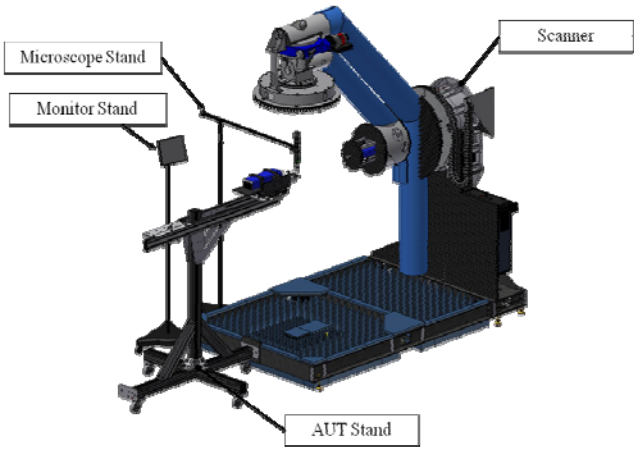

Figure 3. Robotic positioning system

C. *RF system*

The RF sub-system is based on millimeter-wave extension module from OML [8]. A distributed architecture is utilized so as to minimize path loss and therefore maximize the RF link budget. A first module is placed directly after the AUT as shown in figure 4. The connection between the RF probe and the module is realized using WR10 waveguide. Up to 110 GHz, coaxial and waveguide technique coexist, but WR10 has been chosen because of lower loss. In order to use a waveguide connection, a 4-axis XYZ+Tilt module positioner needs to be used. The second millimeter head is placed just behind the probe in the rotational arm. The distance between the AUT and the probe is 587 mm. With this configuration, a signal to noise ratio of 45 dBi is estimated for a 0dBi antenna at 90GHz for 1KHz IF bandwidth.

Figure 4. Low scattering, minimum blockage AUT probing system with millimeter head extension and waveguide connection

III. FAR-FIELD MEASUREMENT

A reference antenna was used for measurement. A single layer simple structure was chosen for accurate simulation. Interaction between AUT and probe is maximal for antenna radiating on the same side as the probe. This is the case of every AoC structure and we decide to select a structure with this type of radiation.

A. Test antenna

In order to have a single-layer structure, a patch type structure was used. To avoid any surface wave excitation, the antenna was realized on a 0.125mm-thick duroid substrate. The susbtrate wavelength (λg) at 90GHz is about 2.2mm, and the patch has a length close to λg/2, which is classical for the first mode of a patch (Figure 5). Patch structure need to be fed using a microstrip line. However, RF probe enable only coplanar connection, then a transition between coplanar and microstrip mode was integrated in the design. An inset feed was realized to match the patch antenna to 50Ω.

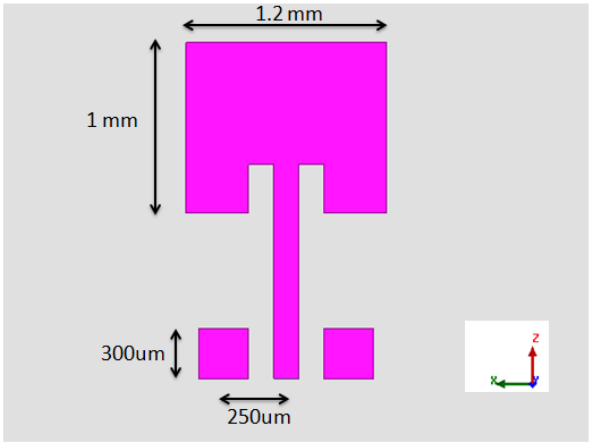

Figure 5. Patch dimensions

This transition is optimized by tuning the size of the ground pad. The pitch of the GSG pad was optimized for a 250um pitch. A picture of the realized prototype connected with the RF probe is presented in Figure 6. The size of the ground plane is 12x10mm².

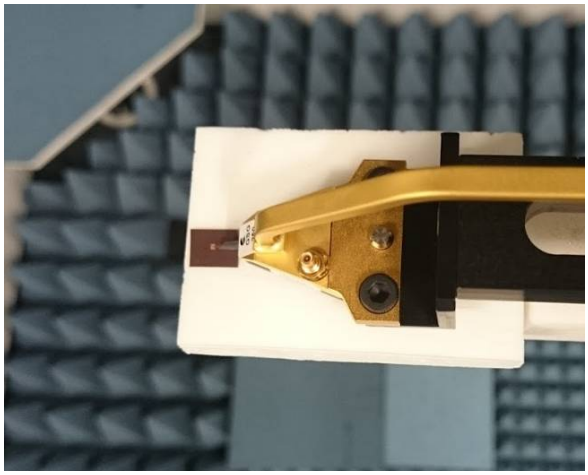

Figure 6. Patch antenna connected with a 250um RF probe

B. Prototype measurement

A far-field measurement was realized using the robotic articulated spherical arm system. The AUT was scanned for a phi variation from -90° to 90° and theta variation from -140° to 140°. This corresponds to a coverage of 88° of the total surface of the sphere. The distance between the AUT and the probe is 587 mm. A comparison between far-field normalized theta gain simulation and measurement is presented on Figure 7 with a 30dB of dynamic. A first order agreement is observed between simulation and measurement. However, large ripples are obtained, especially for a theta variation.

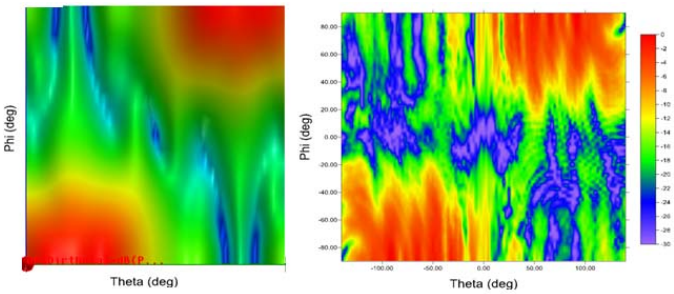

Simulation Measurement

Figure 7. Amplitude comparison between simulation and measurement

E-plane of the patch (yOz) is presented in Figure 8. Many scattering effects due to the probe are observed in this plane. For theta > 120°, amplitude level is attenuated due to the masking (*i.e.* blockage) effect of the probe. Very large ripples (5 to 10 dB) are measured, confirming the fact that interaction with the feeding part is very high.

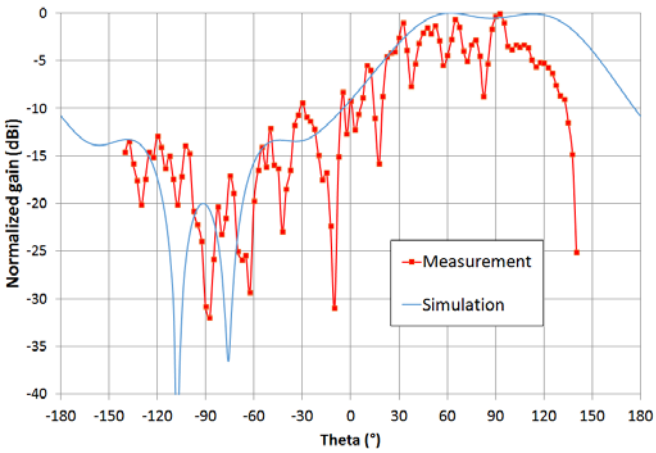

Figure 8. Measured (red trace) and simulated (blue trace) normalized theta gain in yOz plane (E plane)

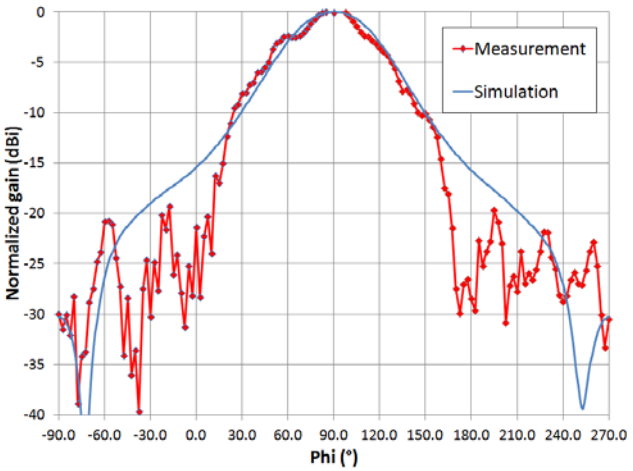

Figure 9. Measured and simulated normalized phi gain in xOy plane (H plane)

H-plane of the patch (xOy) is presented on Figure 9. A better agreement is found with simulation because scattering from the probe is weaker in this plane. This first measurement clearly show the limits for far-field measurement of probed fed antenna with radiating field on the side of the probe. Additional processing would be needed to improve measurement quality.

IV. NEAR-FIELD MEASUREMENT

An important motivation for the design of this set-up is the measurement of the phase on spherical scanning surface. The next section will study the possibility to leverage phase acquisition on probe fed antenna to filter scattering effects.

A. *Phase acquisition challenge*

As its core, the standard spherical near-field theory includes the requirement to accurately and precisely know the phase of the electric near-fields. The comparatively short wavelengths associated with mm-wave and sub-mm-wave testing places very significant demands upon the positional accuracies of the robotic-positioners as well as the stability of the guided wave path. This stability is required both as a function of time for the duration of the near-field acquisition and as a function of position as the probe traverses the spherical sampling surface. Thermal stability is preserved by means of short acquisition times, the use of modern heating ventilation & air-conditioning systems (HVAC), and through the use of return to point calibrations using the patented single point motion tracking interferometry method [8]. Each rotation stage is provided with an integrated RF rotary joint in order to maximize the stability of the guided wave path. The accuracy of the mechanical positioning system is achieved through the careful design utilizing structural analysis [7] and through the use of on the fly structure, *i.e.* droop, correction techniques. However, at the upper end of in the 90 – 110 GHz band the radial uncertainty reported above of ±1.2 mm still translates to ± 158° of electrical phase and this does not include any additional impact resulting from changes in phase of the RF guided wave path. Thus, as it has been established through computational electromagnetic simulation that the radial error is the most critical for SNF testing a novel radial phase correction technique, that utilizes the aforementioned laser tracker co-ordinate measurement data, is utilized to further improve the phase stability of the test system thereby increasing the upper frequency limit of the SNF test system [7].

B. *Near-field measurement of the patch*

A comparison for the phase between simulation and measurement is presented in Figure 10. Using laser alignment system, the exact offset position of the AUT from the sphere center was determined and included in simulation. A fair agreement is observed between measurement and simulation.

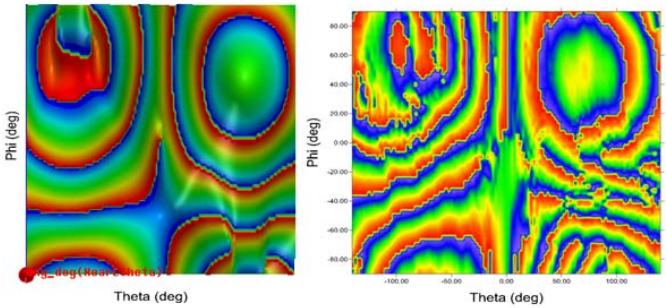

Simulation Measurement

Figure 10. Phase comparison between simulation and measurement

In order to highlight the mechanical deviation during a spherical scanning, the phase on yOz plane is presented in Figure 11. for phi=-90° and phi = 90°. Without any correction, a maximum error of 80° of obtained for theta=90° and -90°.

C. *Radial correction exemple*

As explained in Section II.A, a phase correction can be applied to the measured SNF data to remove the phase impact of the structural variation. Results of the phase on yOz plane for copolarisation and crosspolarisation are presented with and without correction in Figure 11. After applying the radial correction, the maximal phased error between the theta=90° and -90° cases is reduced to 30°.

From this near-field measurement, a near-field to far-field transformation is realized with and without radial correction (Figure 12 and 13). The truncated part of the measurement is set to zero. When we truncate a near-field measurement, we are essentially setting the tangential components of the electric fields over the truncated portion of the sampling surface to zero. This means that we have in effect introduced a perfect electrical conductor (PEC) into that part of the surface.

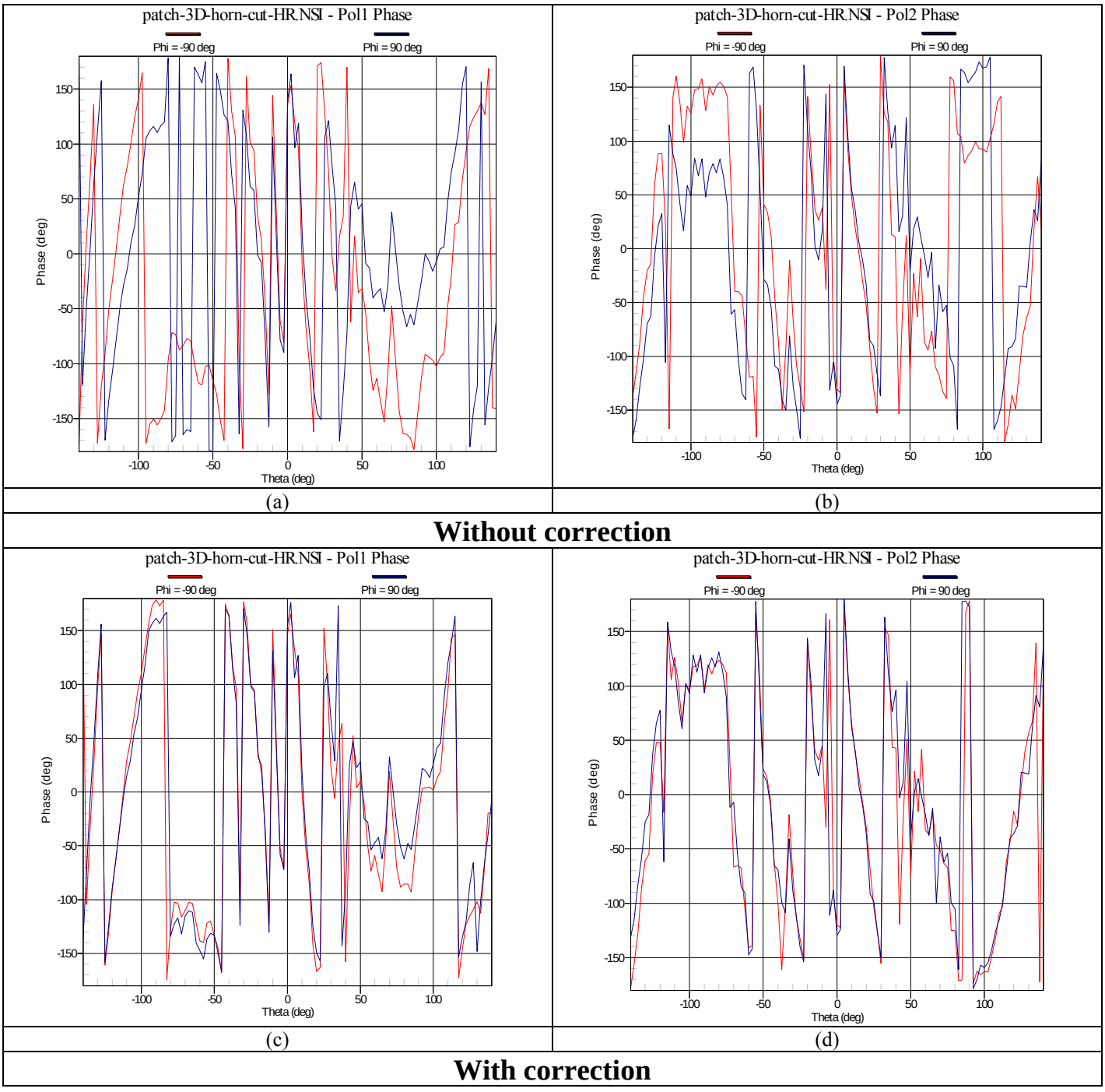

Figure 11. Near field phase on yOz plane for phi=-90° (red) and phi=90° (blue) with and without correction for Copol (a and c) and Crosspol (b and d)

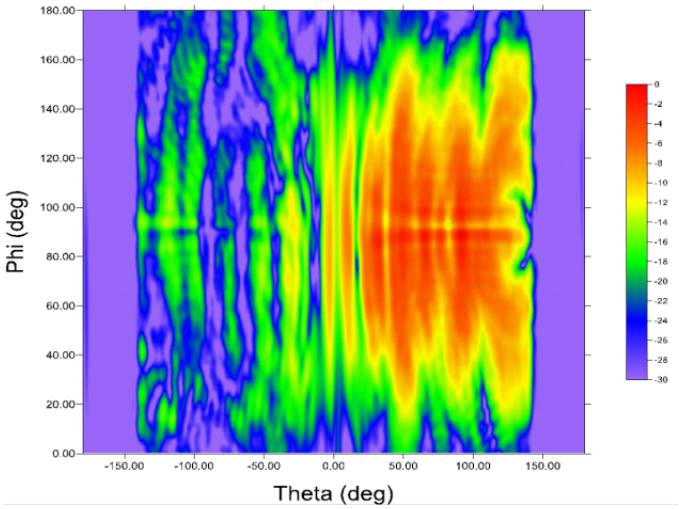

Figure 12. Far-field transformation from Near-Field measurement without radial correction

The sharp discontinuity that can be experienced at the edge of the acquisition interval can lead to spurious high frequency ripping in the transformed far-field pattern as a result of spherical mode leakage. This can be more of an issue when acquiring low gain antennas when it is not possible. Here, considering the radiation pattern of the test antenna, as shown on Figure 8, an important part of the main beam is not measured because of masking of the probing part. In this case the general characteristics of the far-field pattern are similar to the measured fields as the scanning probe is in the quasi far-field of the antenna. The spherical near-field theory is valid at any range length, outside the reactive near-field region and as such it can be applied to this example.

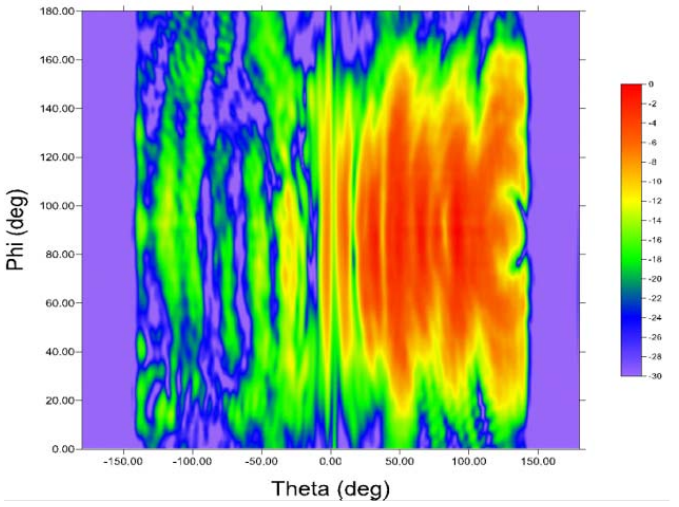

Figure 13. Far-field transformation from Near-Field measurement with radial correction

In the far-field results without any radial correction (Figure 12), an important error is observed for phi = 0°. The test case antenna has a large field intensities right at the seam in the spherical near-field measurement grid making the application of the phase correction to insure continuity of the fields across this artificial boundary particularly important. Any discontinuity would result in the need to use a larger number of higher order spherical modes to match these fields and that can introduce spurious ripple in the resulting transformed far-field pattern, as seen in this example.

In the far-field with radial correction, no discontinuity is observed for phi=90°, resulting in a more accurate radiation pattern.

D. Sperical mode filtering

In this example, a spherical acquisition with a maximum radial extent (MRE) of 25mm was realized. From these results, different far-field transformation with reduced MREs can be performed. The sampling angle for this measurement was 2.5° for theta and phi. For a patch antenna, a MRE equal to two free-space wavelengths (2x λ_0) is usually enough to measure the main spherical modes. At 90GHz, this corresponds to a MRE of 3.3mm. Thus, from this measurement, the near-field to far-field processing could be applied using a smaller MRE. This method will attenuate the random error signals. Filtering for a MRE of 10mm is presented on Figure 14. An attenuation of the fast ripple is observed but the deeper scatterings are not attenuated. For a filtering with a smaller MRE of 5mm (Figure 15), a higher filtering of the ripple is observed. Some field start to appear in the truncated area (theta > 140°), but the radiation pattern is distorted. Using larger MREs results in an increase in the spherical measurement time which is a result of the sampling theorem requiring the acquisition of more finely-spaced spherical samples. Thus using excessively large MREs can be undesirable except for those cases where the additional information obtained can be used to improve the quality of the measurement [10].

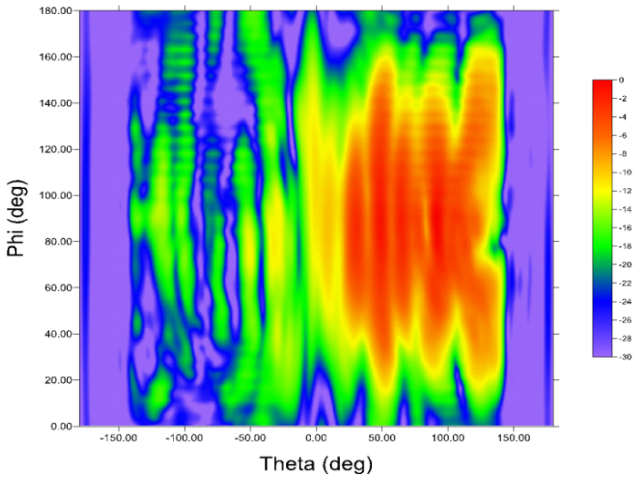

Figure 14. Far-field transformation from Near-Field measurement with radial correction and MRE of 10mm

E. Perspectives

The measurement and post-processing mode orthogonalisation and filtering technique, Mathematical Absorber Reflection Suppression (MARS) [10], has been used

extensively, for over a decade now, to identify and subsequently extract measurement errors arising from spurious scattered fields that are introduced when antenna testing is performed in echoic environments. Underpinning the success of the MARS measurement and post-processing technique is the behavior of the orthogonal spherical vector wave (mode) functions that are employed to describe the radiated fields and in particular their behavior under the isometric co-ordinate translations. As the effectiveness of the mode filtering technique is directly related to the magnitude of the electrical displacement of the test antenna [9], this method is particularly well suited to mm-wave applications where even modest physical displacements correspond to many wavelengths. In this application this is all the more crucial as the articulated SNF system is housed within an open laboratory environment rather than being installed within a more conventional anechoic chamber.

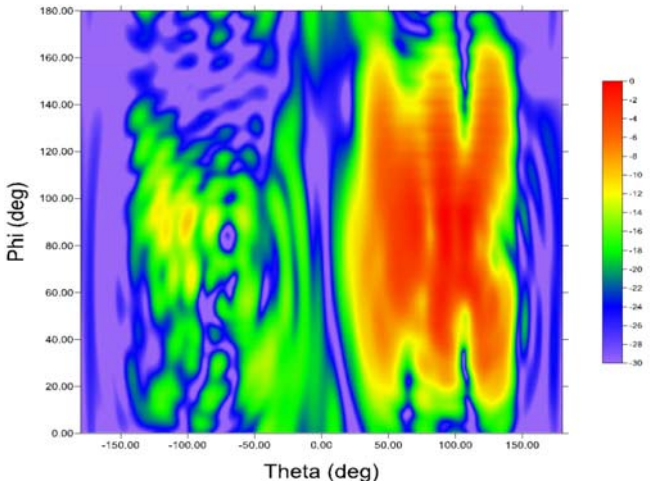

Figure 15. Far-field transformation from Near-Field measurement with radial correction and MRE of 5mm

All previous applications of spherical MARS have involved the AUT being rotated about one or more axes during the course of the acquisition. However here, uniquely, the AUT remains entirely at rest for the duration of the measurement. Although the AUT is stationary, the near-field probe *is* in motion, and therefore the same differential scattering that is seen when using a conventional phi over theta (*i.e.* model tower) spherical positioner is also observed in this case thus allowing the MARS technique to distinguish between those fields that are radiated by the AUT and those that result from range clutter. This observation is true for both the near- and far-field implementations of MARS thereby allowing scattering suppression to be used effectively in either measurement mode. Whilst MARS processing can be performed at a single frequency and only requires a single measurement, scan times can be increased which is a result of the sampling theorem requiring the acquisition of more finely-spaced spherical as a consequence of the increased maximum radial extent. This can be more of an issue for the near-field measurements as two-dimensional data is taken whereas when taking far-field data only a single great-circle cut is required where the scan this increase is negligible. For MARS processing to be entirely successful the AUT displacement should be comparable with the largest dimension of the AUT, however for cases where it is inconvenient or impossible to use such a large translation, some more limited suppression is provided with smaller offsets including the attenuation of random error signals.

V. Summary And Conclusion

This paper presents initial results obtained from a new antenna measurement system specifically implemented for the measurement of probe-fed antenna pattern measurements using a high accuracy spherical articulated arm. Results are presented that illustrate how a laser tracker structural measurement can be utilized to enhance the ability of such scanners for use at higher frequencies. The obvious requirement in this instance is that the structure motion be time invariant since the correction technique will not be valid otherwise. Higher mode spherical filtering has marginally improved measured results. In order to filter RF probe scattering is a more efficient way a mode advanced post-processing technique could be used and this is an area of ongoing research.

Acknowledgement

F. Devillers from Orange is acknowledged for the fabrication of the core foam support in the frame of the CREMANT.

References

[1] D. Titz , F. Ferrero , C. Luxey, “Development of a Millimeter-Wave Measurement Setup and Dedicated Techniques to Characterize the Matching and Radiation Performance of Probe-Fed Antennas”, IEEE Antennas and Propagation Magazine, Vol. 54, pp. 188-203, 2012.

[2] H. Gulan, S. Beer, C. Rush, A. Leuther, I. Kalfass, T. Zwick, “Probe based antenna measurements up to 325 GHz for upcoming millimeter-wave applications”, International Workshop on Antenna Technology (iWAT), pp. 228-231, 2013

[3] F. Manzillo, R. Nastri, M. Spella, G. Gentile, M. Spirito, "A 60-GHz Passive Broadband Multibeam Antenna System in Fused Silica Technology," Antennas and Wireless Propagation Letters, IEEE , vol.12, no., pp.1376,1379, 2013

[4] P. Padilla, P. Pousi, A. Tamminen, J. Mallat, L. Ala-Laurinaho, M. Sierra-Castaner, A.V. Raisanen, "Experimental Determination of DRW Antenna Phase Center at mm-Wavelengths Using a Planar Scanner: Comparison of Different Methods," Antennas and Propagation, IEEE Transactions on , vol.59, no.8, pp.2806,2812, Aug. 2011

[5] L. Boehm, F. Boegelsack, M. Hitzler, C. Waldschmidt, “An Automated Millimeter-Wave Antenna Measurement Setup Using a Robotic Arm”, APS 2015, Vancouver, Canada

[6] E. Lee, R. Soerens, E. Szpindor, P. Iversen, “Challenges of 60 GHz On-Chip Antenna Measurements”, IEEE APS 2015, Vancouver, Canada,

[7] D. J. V. Rensburg, “Factors Limiting the Upper Frequency of mm-Wave Spherical Near-field Test Systems”, Eucap 2015, Lisbon, Portugal

[8] OML Inc, 300 Digital Drive Morgan Hill, CA 95037

[9] D. Slater, “Three -Axis Motion Tracking Interferometer For Measurement and Correction of Positional Errors Between an Article Under Test and a Measurement Probe”, United States Patent number 5,419,631.

[10] C.G. Parini, S.F. Gregson, J. McCormick, D. Janse van Rensburg “Theory and Practice of Modern Antenna Range Measurements”, IET Press, 2014, ISBN 978-1-84919-560-7.